11-2017

Mito-Apocynin Prevents Mitochondrial Dysfunction, Microglial Activation, Oxidative Damage, and Progressive Neurodegeneration in MitoPark Transgenic Mice

Monica Langley
Iowa State University

Anamitra Ghosh
Iowa State University

Adhithiya Charli
Iowa State University

Souvarish Sarkar
Iowa State University

Muhammet Ay
Iowa State University

See next page for additional authors

Antioxidants & Redox Signaling, Vol. 27, No. 14 (November 2017) : 1048-1066. DOI.

Mito-Apocynin Prevents Mitochondrial Dysfunction, Microglial Activation, Oxidative Damage, and Progressive Neurodegeneration in MitoPark Transgenic Mice

Monica Langley
Department of Biomedical Sciences, Iowa Center for Advanced Neurotoxicology, Iowa State University, Ames, Iowa
Anamitra Ghosh
Department of Biomedical Sciences, Iowa Center for Advanced Neurotoxicology, Iowa State University, Ames, Iowa
Adhithiya Charli
Department of Biomedical Sciences, Iowa Center for Advanced Neurotoxicology, Iowa State University, Ames, Iowa
Souvarish Sarkar

Department of Biomedical Sciences, Iowa Center for Advanced Neurotoxicology, Iowa State University, Ames, Iowa

Muhammet Ay

Department of Biomedical Sciences, Iowa Center for Advanced Neurotoxicology, Iowa State University, Ames, Iowa

Jie Luo

Department of Biomedical Sciences, Iowa Center for Advanced Neurotoxicology, Iowa State University, Ames, Iowa

Jacek Zielonka

Department of Biophysics, Medical College of Wisconsin, Milwaukee, Wisconsin

Timothy Brenza

Department of Chemical and Biological Engineering, Iowa State University, Ames, Iowa

Brian Bennett

Department of Physics, Marquette University, Milwaukee, Wisconsin

Huajun Jin

Department of Biomedical Sciences, Iowa Center for Advanced Neurotoxicology, Iowa State University, Ames, Iowa

Shivani Ghaisas

Department of Biomedical Sciences, Iowa Center for Advanced Neurotoxicology, Iowa State University, Ames, Iowa

Benjamin Schlichtmann

Department of Chemical and Biological Engineering, Iowa State University, Ames, Iowa

Dongsuk Kim

Department of Biomedical Sciences, Iowa Center for Advanced Neurotoxicology, Iowa State University, Ames, Iowa

Vellareddy Anantharam

Department of Biomedical Sciences, Iowa Center for Advanced Neurotoxicology, Iowa State University, Ames, Iowa

Arthi Kanthasamy

Department of Biomedical Sciences, Iowa Center for Advanced Neurotoxicology, Iowa State University, Ames, Iowa

Balaji Narasimhan

Department of Chemical and Biological Engineering, Iowa State University, Ames, Iowa

Balaraman Kalyanaraman

Department of Biophysics, Medical College of Wisconsin, Milwaukee, Wisconsin

Anumantha G. Kanthasamy

Department of Biomedical Sciences, Iowa Center for Advanced Neurotoxicology, Iowa State University, Ames, Iowa

Abstract

Aims: Parkinson's disease (PD) is a neurodegenerative disorder characterized by progressive motor deficits and degeneration of dopaminergic neurons. Caused by a number of genetic and environmental factors, mitochondrial dysfunction and oxidative stress play a role in neurodegeneration in PD. By selectively knocking out mitochondrial transcription factor A (TFAM) in dopaminergic neurons, the transgenic MitoPark mice recapitulate many signature features of the disease, including progressive motor deficits, neuronal loss, and protein inclusions. In the present study, we evaluated the neuroprotective efficacy of a novel mitochondrially targeted antioxidant, Mito-apocynin, in MitoPark mice and cell culture models of neuroinflammation and mitochondrial dysfunction.

Results: Oral administration of Mito-apocynin (10 mg/kg, thrice a week) showed excellent central nervous system bioavailability and significantly improved locomotor activity and coordination in MitoPark mice. Importantly, Mito-apocynin also partially attenuated severe nigrostriatal degeneration in MitoPark mice. Mechanistic studies revealed that Mito-apo improves mitochondrial function and inhibits NOX2 activation, oxidative damage, and neuroinflammation.

Innovation: The properties of Mito-apocynin identified in the MitoPark transgenic mouse model strongly support potential clinical applications for Mito-apocynin as a viable neuroprotective and anti-neuroinflammatory drug for treating PD when compared to conventional therapeutic approaches.

Conclusion: Collectively, our data demonstrate, for the first time, that a novel orally active apocynin derivative improves behavioral, inflammatory, and neurodegenerative processes in a severe progressive dopaminergic neurodegenerative model of PD. Antioxid. Redox Signal. 27, 1048–1066.

Keywords

mitochondria, Parkinson’s disease, Mito-apocynin, apocynin, neuroprotection

Introduction

Parkinson's disease (pd) is a debilitating neurodegenerative disorder, affecting millions of people worldwide and is triggered by a complex interplay of genetic and environmental factors. PD neuropathology is characterized by a loss of dopaminergic neurons in the substantia nigra (SN), loss of dopamine (DA) in the striatum, and accumulation of abnormal α-synuclein protein, a major constituent of Lewy bodies and Lewy neurites (63). Motor symptoms such as bradykinesia, tremor, rigidity, and postural instability are still used to clinically diagnose PD. Although it is known that neuronal loss leads to DA deficiency and motor dysfunction, less is understood regarding the mechanisms underlying the loss of SN neurons (55). Neuroinflammation, oxidative stress, and mitochondrial dysfunction have all been implicated in PD pathogenesis (65, 68). Although mitochondrial dysfunction is well established as an overriding pathophysiological indication of PD, no effective treatment options are available to improve the efficiency of mitochondrial function in PD.

Innovation

Advances in drug discovery for neurodegenerative diseases have been hampered by the lack of models that recapitulate the chronic, progressive neurodegeneration characteristic of Parkinson's disease (PD). However, a recently developed genetic model of mitochondrial dysfunction, known as MitoPark mice, mirrors many key features of PD. Recently, we developed a new class of pharmacological agents to effectively dampen the major pathophysiological processes associated with PD (19). The properties of

Mito-apocynin identified in this model strongly support potential clinical applications for Mito-apocynin as a viable neuroprotective and antineuroinflammatory drug for treating PD when compared to conventional therapeutic approaches.

Mitochondrial toxin-based PD models such as 1-methyl-4-phenyl-1,2,3,6-tetrahydropyridine (MPTP), 6-hydroxydopamine (6-OHDA), and rotenone are used to screen compounds for further development. However, toxin-based PD models do not reflect human PD mainly due to the acute nature of neuronal injury, toxicant/drug interactions, and between-subject response variation (6, 21, 47). MitoPark mice were created by selective inactivation of mitochondrial transcription factor A (TFAM) in the nigrostriatal pathway (22). Key pathological features of PD such as adult onset, progressive neurodegeneration, protein inclusions, and progressive motor deficits ameliorated by l-3,4-dihydroxyphenylalanine (l-DOPA) have been identified in MitoPark mice (27), making the model ideal for testing novel mitochondria-targeted neuroprotective agents.

A strong therapeutic potential exists for mitochondria-targeted antioxidants (MTAs) in neurodegenerative disorders (39). We recently demonstrated that apocynin (4-hydroxy-3-methoxyacetophenone), a plant-derived molecule structurally related to vanillin, and its dimer, diapocynin, are neuroprotective in the MPTP and LRRK2^{R1441G} mouse models (18, 32). As an inhibitor of NOX2 activity, apocynin has been studied in various cell culture and animal models of PD (1, 12, 28). Although the high doses of apocynin and diapocynin (300 mg/kg) used in these animal studies were well tolerated, more efficacious apocynin analogs are needed. We therefore synthesized a series of mitochondria-targeted apocynins (conjugated to a triphenylphosphonium cation moiety via an alkyl chain with differing chain lengths [C_2-C_{11} carbon atoms]). Using Mito-apo-C_2, we have recently established that Mito-apo protected against neuroinflammation and neurodegeneration in the MPTP model (33). Herein, we evaluated the disease-modifying efficacy of a long-acting Mito-apo-C_{11} in the MitoPark model that recapitulates key features of PD, including mitochondrial dysfunction, microglial activation, and dopaminergic degeneration. Our results show that oral administration of Mito-apo dampens chronic, progressive behavioral deficits and dopaminergic neurodegeneration. Additional mechanistic studies support the enhanced mitochondrial function and anti-inflammatory properties of Mito-apo.

Results

Mito-apo restores mitochondrial function in dopaminergic neuronal cells

We first assessed the effect of Mito-apo on key markers of mitochondrial bioenergetics of dopaminergic neuronal cells. The Seahorse extracellular flux analyzer revealed the basal respiration rate to be nearly double the control oxygen consumption rate (OCR) values in 10- to 30-μM Mito-apo-treated N27 dopaminergic neuronal cells (Fig. 1A, B). On treatment with oligomycin, Mito-apo-treated cells showed a significantly higher ATP-linked respiration (Fig. 1A, C) and respiratory capacity (Fig. 1A, D) than untreated cells. As expected, in the positive control, 1 μM rotenone abolished the OCR signal (Fig. 1A–D).

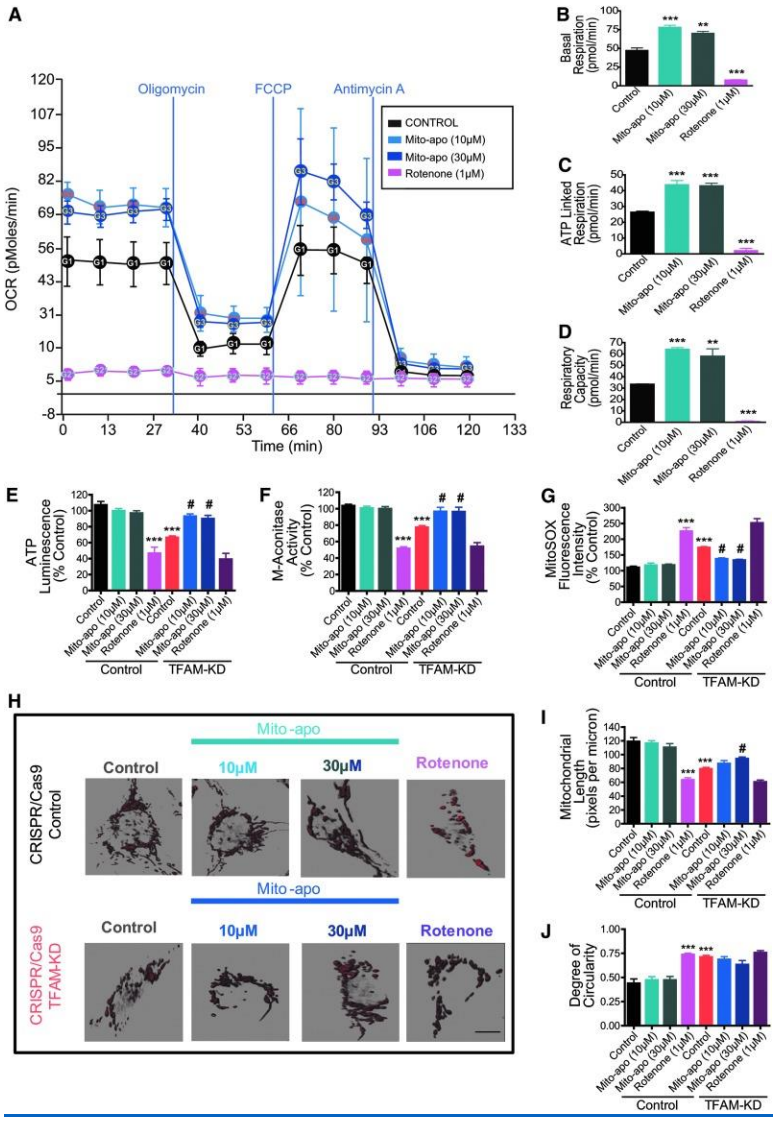

FIG. 1. Bioenergetics and *in vitro* characterization of Mito-apo. (A–D) N27 cells given 10–30 μM Mito-apo for 3 h were measured using a Seahorse XF96 analyzer. Basal respiration rate before injection **(A, B)**. After adding oligomycin, ATP-linked respiration **(A, C)**. Respiratory capacity measured as OCR after carbonilcyanide p-trifluoromethoxyphenylhydrazone (FCCP) injection **(A, D)**. **(E–G)** Mito-apo replenished ATP levels, **(E)** upregulated *m*-aconitase activity, **(F)** and decreased oxidant production in TFAM KD cells (TFAM-KD). TFAM-KD and control cells were incubated with 10–30 μM Mito-apo for 3 **(E–F)** or 12 h **(G)**. Raw luminescence units of ATP produced **(E)**. Aconitase activity **(F)** and mitochondrial ROS production **(G)** as determined by aconitase and MitoSOX assays. **(H–J)** TFAM-KD and control cells were incubated with 10–30 μM Mito-apo for 12 h, and mitochondria were stained by MitoTracker (scale bar = 10 μm). Analysis of mitochondrial length **(I)** and degree of circularity **(J)**. Rotenone (1 μM) was used as a positive control in all experiments. Graphical results represented as the mean ± SEM ($n = 6$ wells/group). $^{**}p < 0.01$ *versus* control; $^{***}p < 0.001$ *versus* control; $^{\#}p < 0.05$ *versus* vehicle-treated TFAM-KD cells. See also Supplementary Figures S1 and S6. KD, knockdown; OCR, oxygen consumption rate; ROS, reactive oxygen species; SEM, standard error of the mean; TFAM, mitochondrial transcription factor A.

Given that knockdown (KD) of TFAM has been shown to result in cellular ATP depletion and loss of mitochondrial function in mammalian cell culture studies (48), we determined if Mito-apo could improve mitochondrial function in stable TFAM-KD N27 cells that we generated using the CRISPR/Cas9 system as

described in Supplementary Data (Supplementary Data are available online at www.liebertpub.com/ars). Transduction of N27 cells with TFAM-KD resulted in >80% loss in TFAM mRNA levels relative to control cells (Supplementary Fig. S1). In contrast to control N27 cells, TFAM-KD cells had significantly lower cellular ATP levels (Fig. 1E). Rotenone (1 μM) for 3 h (positive control) dramatically decreased cellular ATP levels in control N27 cells. Mito-apo did not significantly alter the ATP levels in control cells. However, exposure to 10–30 μM Mito-apo for 3 h dramatically increased cellular ATP levels in TFAM-KD N27 cells, suggesting that Mito-apo replenishes ATP levels in mitochondrially stressed cells.

Aconitases are iron–sulfur-containing enzymes that isomerize citrate and are inactivated during mitochondrial oxidative stress. Measurement of aconitase enzyme activity in TFAM-KD cells revealed significantly decreased *m*-aconitase activity when compared to control N27 cells, indicating that TFAM-KD led to significant mitochondrial oxidative damage (Fig. 1F). However, treating the TFAM-KD cells with 10–30 μM Mito-apo for 3 h returned *m*-aconitase activity to levels present in control N27 cells. Mito-apo did not significantly alter the *m*-aconitase activity in control cells, and rotenone strongly reduced *m*-aconitase activity in both cells (Fig. 1F).

We also assessed the loss of mitochondrial function with MitoSOX™ red dye in TFAM-KD and control N27 cells. Basal oxidation of MitoSOX probe was significantly higher in TFAM-KD than in control cells (Fig. 1G). A 12-h exposure to 10 and 30 μM Mito-apo decreased the rate of probe oxidation in TFAM-KD, but not in control N27 cells (Fig. 1G). As observed previously using hydroethidine probe in control N27 cells (20), rotenone strongly stimulated MitoSOX oxidation in both cell lines.

MitoTracker red dye was used to visualize integrity or structural abnormalities in TFAM-KD N27 cells. Healthy mitochondria, such as those from control cells, appear as long, thread-like structures (Fig. 1H). Relative to those of control cells, the mitochondria of TFAM-KD N27 cells were significantly shorter (Fig. 1I) and more circular (Fig. 1J), further indicating a striking loss of mitochondrial structural integrity. Although 10 μM Mito-apo was not enough to improve mitochondrial morphology, TFAM-KD cells treated with 30 μM Mito-apo exhibited significantly increased mitochondrial length (Fig. 1H, I). Collectively, results from these experiments suggest that Mito-apo restores mitochondrial morphology and function in TFAM-KD N27 cells.

Mito-apo stalls progression of motor deficits

Considering that Mito-apo was capable of replenishing mitochondrial function in TFAM-KD N27 cells, we decided to determine if Mito-apo is neuroprotective in the MitoPark mouse model of PD, in which TFAM is selectively inactivated in dopaminergic neurons. Preceded by early neurochemical alterations, these mice exhibit behavioral deficits by 12 weeks, which become progressively worse by 24 weeks (34). Our dose for this study was initially based on the severity of our model and the therapeutic efficacy reported for other model systems in previous publications (19, 33). Given that MitoPark is one of the most severe models of PD, we considered that the lower dose of Mito-apocynin used in the MPTP article (3 mg/kg/day) and LRRK2 article (3 mg/kg, 3 × /week) might not be sufficient in the MitoPark mice, and therefore used a higher dose. As depicted in our treatment paradigm (Fig. 2A), MitoPark and age-matched C57 mice were orally administered either Mito-apo (10 mg/kg, 3 × /week) or vehicle (10% ethanol/PBS) beginning at age 13 weeks. Open-field activity and rotarod behavioral performances were evaluated at ages 18, 21, and 24 weeks (Supplementary Fig. S2).

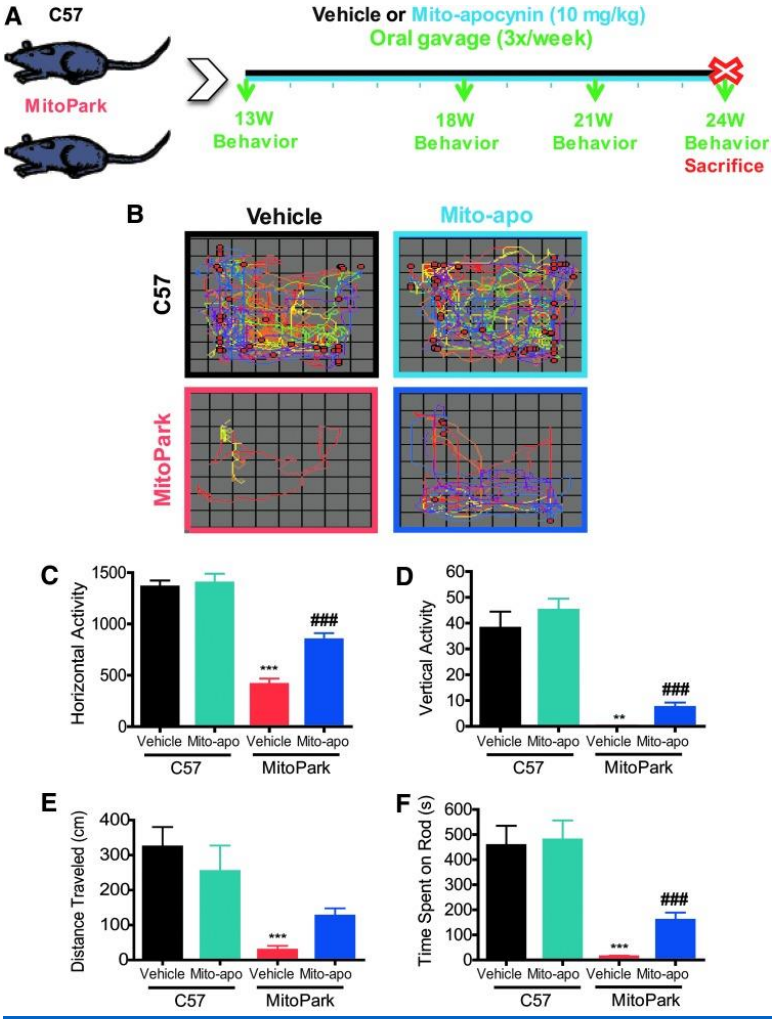

FIG. 2. Progressive motor deficits in MP mice are improved with Mito-apo. (A) Treatment schedule showing C57 and MP mice orally administered vehicle or Mito-apo (10 mg/kg). **(B)** VersaPlot showing horizontal activity and rearing activity (*red dots*) during a 10-min open-field test. Horizontal **(C)** and vertical **(D)** activities and distance traveled **(E)** during open-field test. **(F)** Time spent on rotarod. Graphical results represented as the mean ± SEM (n = 9–13 mice/group). $^{**}p < 0.01$ *versus* control; $^{***}p < 0.001$ *versus* control; $^{\#\#\#}p < 0.001$ *versus* vehicle-treated MP. See also Supplementary Figure S2. MP, MitoPark.

Decreased movement, as expected in 24-week MitoPark mice, is shown by representative Versaplot maps (Fig. 2B), and improved locomotion can be seen in plots of the Mito-apo-treated MitoPark mice. Consistently, 24-week MitoPark mice exhibited decreased horizontal activity (Fig. 2C), vertical activity (Fig. 2D), total distance traveled (Fig. 2E), and time spent on the rotarod (Fig. 2F). Mito-apo treatment did not have any significant effect on any of these behavioral parameters in age-matched control mice, but importantly, the horizontal and vertical activity levels and rotarod performance of MitoPark mice were significantly retained by Mito-apo treatment in contrast to vehicle-treated MitoPark mice.

Mito-apo treatment dampens nigrostriatal tyrosine hydroxylase neuronal loss and striatal DA depletion

Neurodegeneration in the SN is progressive and severe in aged MitoPark mice (27). Brain sections from 24-week MitoPark mice were immunostained for tyrosine hydroxylase (TH) to detect dopaminergic neurons. A significant

loss of TH^+ cell bodies and terminals in the SN and striatum, respectively, occurred in vehicle-treated 24-week MitoPark mice (middle panel) in contrast to vehicle-treated age-matched C57 mice (top panel) (Fig. 3A). DAB immunostaining showed significantly higher levels of TH immunoreactivity (Fig. 3A) and neuronal counts (Fig. 3B) in the striatum and SN of Mito-apo-treated MitoPark mice compared to vehicle-treated MitoPark mice. Mito-apo did not alter the number of TH neurons in control mice. Further confirmation came from Western blots and their densitometric analysis, where higher levels of TH protein expression were observed in the SN of Mito-apo-treated MitoPark mice *versus* vehicle-treated MitoPark mice (Fig. 3C). Full Western blots from cropped images in all figures can be found in Supplementary Fig. S3.

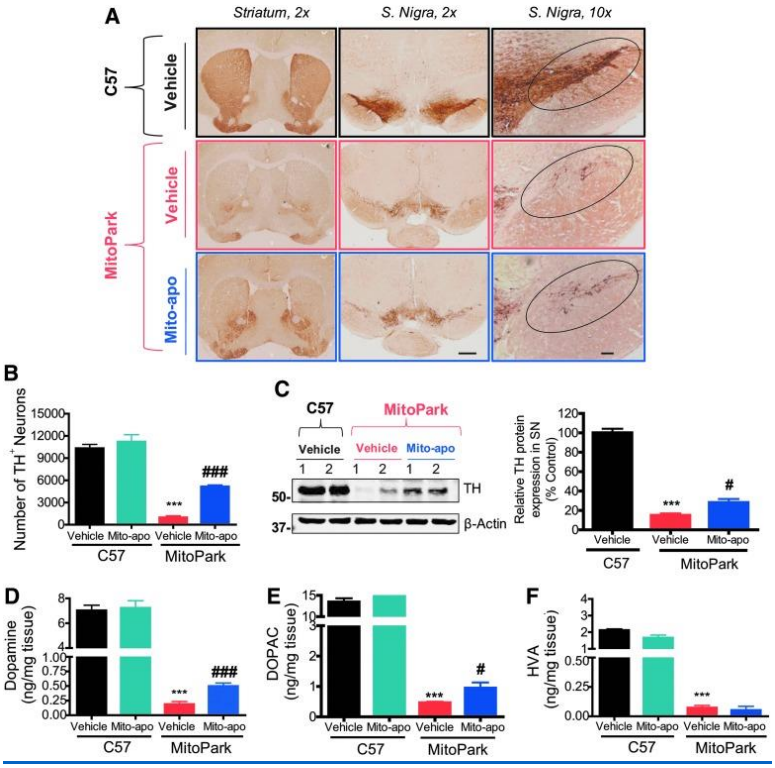

FIG. 3. Neurodegeneration and dopamine depletion in MP mice are attenuated by Mito-apo. DAB immunostaining **(A)** in striatum and SN (scale bars = 1 mm and 100 µm) of vehicle-treated C57 (*top*), vehicle-treated MP (*middle*), and Mito-apo-treated MP mice (*bottom*). **(B)** Stereological cell counts of TH^+ neurons in the SN of $n = 3$/group. **(C)** Representative Western blot of two animals/group and densitometric analysis of TH protein levels normalized to β-actin in the SN ($n = 6$/group). High-performance liquid chromatography with electrochemical detection was used for determination of dopamine **(D)**, DOPAC **(E)**, and HVA **(F)**. Graphical results represented as the mean ± SEM ($n = 6$–8 mice/group). $^{***}p < 0.001$ *versus* vehicle-treated C57; $^{\#}p < 0.05$, or $^{\#\#\#}p < 0.001$ *versus* vehicle-treated MP. DOPAC, 3,4-dihydroxyphenylacetic acid; HVA, homovanillic acid; SN, substantia nigra; TH, tyrosine hydroxylase.

Since Mito-apo-treated MitoPark mice had more dopaminergic neurons remaining in the SN, we performed high-performance liquid chromatography (HPLC) with electrochemical detection to determine if striatal levels of DA and its metabolites were also protected. We observed a severe loss of DA, DOPAC, and HVA, respectively, in the striatum of vehicle-treated MitoPark mice compared to age-matched control mice (Fig. 3D–F). In contrast, Mito-apo increased DA and DOPAC by 2.6- and 2.0-fold, respectively, when compared to vehicle-treated MitoPark mice. Mito-apo did not affect striatal DA and its metabolite levels in C57 black mice. Together, these

data suggest that Mito-apo substantially increases the TH neuronal cell count and striatal DA levels in aged MitoPark mice.

Mito-apo attenuates mitochondrial aconitase inactivation and oxidative damage

To further determine the effect of Mito-apo on mitochondrial redox status in the MitoPark model, we used *ex vivo* electron paramagnetic resonance (EPR) analysis to see if Mito-apo protects against inactivation of mitochondrial aconitase. Previously, we had shown that Mito-Q_{10} treatment mitigates MPTP-mediated inactivation of mitochondrial aconitase and inhibits the increase in the EPR signal intensity at $g' = 6$ (attributed to cytochrome c) detected in brain tissues obtained from MPTP-treated mice (31). Similarly, in this study, we show that the EPR spectra in the $g \sim 2$ region (blue bracket, Fig. 4A) from MitoPark striatal samples (middle spectra, Fig. 4B) have higher fractional intensities, which are primarily due to the inactive, oxidized $[3Fe–4S]^+$ cluster of aconitase. EPR spectral signals were internally normalized to high-spin heme (blue arrow, Fig. 4A, C). A similar trend occurred in cortical tissues, but was insignificant (Supplementary Fig. S4). Most importantly, Mito-apo treatment significantly reduced the fractional intensities from the $[3Fe–4S]^+$ cluster signal in MitoPark mice relative to vehicle treatment (Fig. 4D).

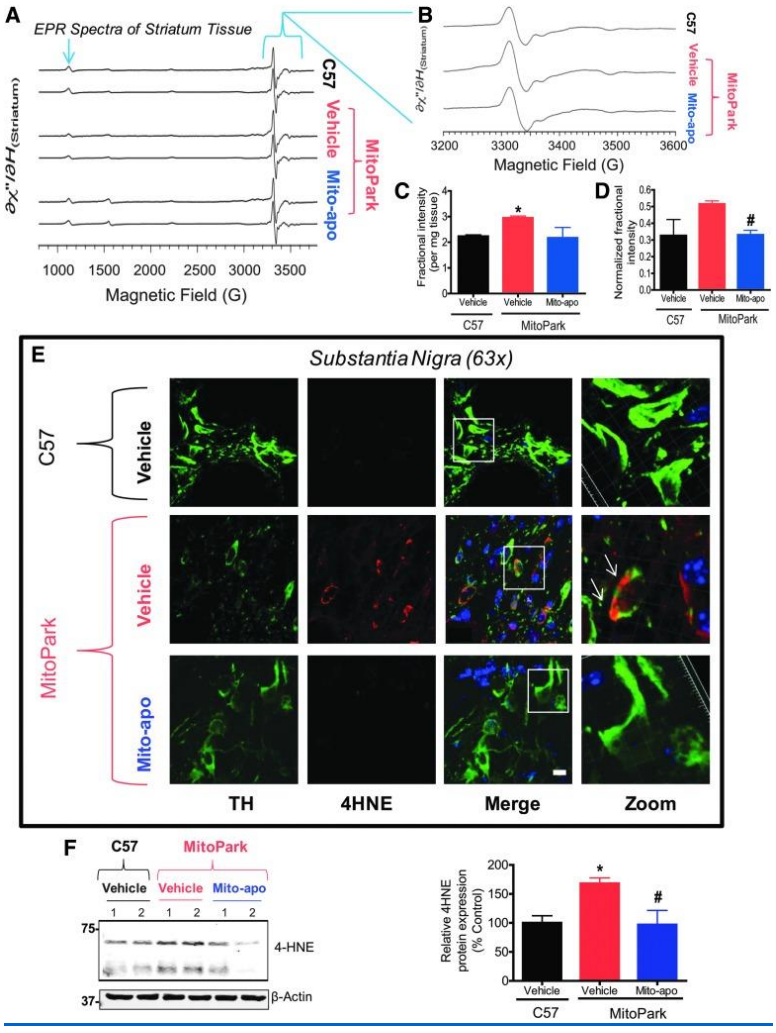

FIG. 4. Mitochondrial aconitase inactivation and oxidative stress are attenuated in Mito-apo-treated MP mice. **(A)** The $g \sim 2$ region (*blue bracket*) and HS heme (*arrow*, internal control) of the experimental EPR spectra from the pooled striatum (each spectrum represents 3–5 combined animal tissues) from vehicle-treated C57 (*top*), vehicle-treated MP (*middle*), and MP mice treated with 10 mg/kg Mito-apo from 13 to 24 weeks of age

(*bottom*). The spectra are primarily due to the oxidized [3Fe–4S] cluster of aconitase (~3330 G), and the reduced N2 (3370 G), N4 (3485 G), and N3 (3540 G) complex I iron–sulfur complexes, although other components underlie these species, and fits to all components were used to estimate the relative contributions to the spectra (fits are presented under each of the three experimental traces, respectively, in **A**). **(B)** Expansion of the $g \sim 2$ region. Fractional intensities from EPR spectra in the $g \sim 2$ region normalized to combined tissue weight **(C)** and internally normalized to the HS-heme group **(D)**. **(E)** Twenty-four-week mouse tissues of vehicle-treated C57 (*top*), vehicle-treated MP (*middle*), and Mito-apo-treated MP mice (*bottom*) were double immunostained for TH and 4-HNE (scale bar = 10 μm). Merged MP image shows colocalization of TH and 4-HNE in DAergic neurons. **(F)** Representative Western blot and densitometric analysis of 4-HNE protein in the SN (n = 6/group). $^{*}p < 0.05$ *versus* C57; $^{\#}p < 0.05$ *versus* vehicle-treated MP. See also Supplementary Figure S4. EPR, electron paramagnetic resonance; 4-HNE, 4-hydroxynonenal.

Oxidative damage biomarkers such as nitrotyrosine-containing proteins and lipid peroxidation product 4-hydroxynonenal (4-HNE) have been shown in animal models of PD and have high correlation to disease states (32, 51). Confocal imaging of immunohistochemistry (IHC) double labeled with TH antibody and Western blot analysis revealed increased 4-HNE expression in the SN of aged MitoPark mice but not in control mice (Fig. 4E, F). Mito-apo administration almost completely suppressed 4-HNE levels in the SN of aged MitoPark mice. These results demonstrate that Mito-apo attenuates mitochondrial aconitase inactivation in the striatum and oxidative damage in nigral neurons of aged MitoPark mice.

Mito-apo inhibits microglia activation in the SN

Neuroinflammation is now recognized to play a key role in dopaminergic neurodegeneration in human PD patients and in mouse models (17, 53, 66). Although mitochondrial dysfunction and oxidative stress act as key players in the progressive degenerative MitoPark mouse model, the presence of neuroinflammation in this model has not yet been explored. Western blotting and DAB immunostaining show that IBA1 expression increases in the SN of MitoPark mice (Fig. 5A, B). However, levels of the IBA1 protein were significantly lower in Mito-apo-treated MitoPark mice. IBA1 DAB immunostaining (Fig. 5B) revealed an increased number of microglia in the aged, vehicle-treated MitoPark SN, and at higher magnification, increased soma size and fewer processes, indicating an activated phenotype. These features occurred to a much lesser extent in the Mito-apo-treated MitoPark mice. Indeed, the cell count per field (Fig. 5C) was significantly lower in the Mito-apo-treated group, average soma size was smaller (Fig. 5D), and ImageJ skeleton analysis revealed more process endpoints per cell in Mito-apo-treated MitoPark mice when compared to vehicle-treated MitoPark mice (Fig. 5E). Other variables indicative of a normal microglia phenotype, such as the number of branches, number of junctions, and the longest-shortest path, were significantly reduced in the MitoPark group when compared to controls (Fig. 5F–H). However, the MitoPark mice treated with Mito-apo did not exhibit significant microglial morphological changes when compared to age-matched control mice. We also observed $CD68^{+}$ staining, a marker of microglia activation, in vehicle-treated MitoPark mice that was not present in control or Mito-apo-treated MitoPark mice (Supplementary Fig. S5).

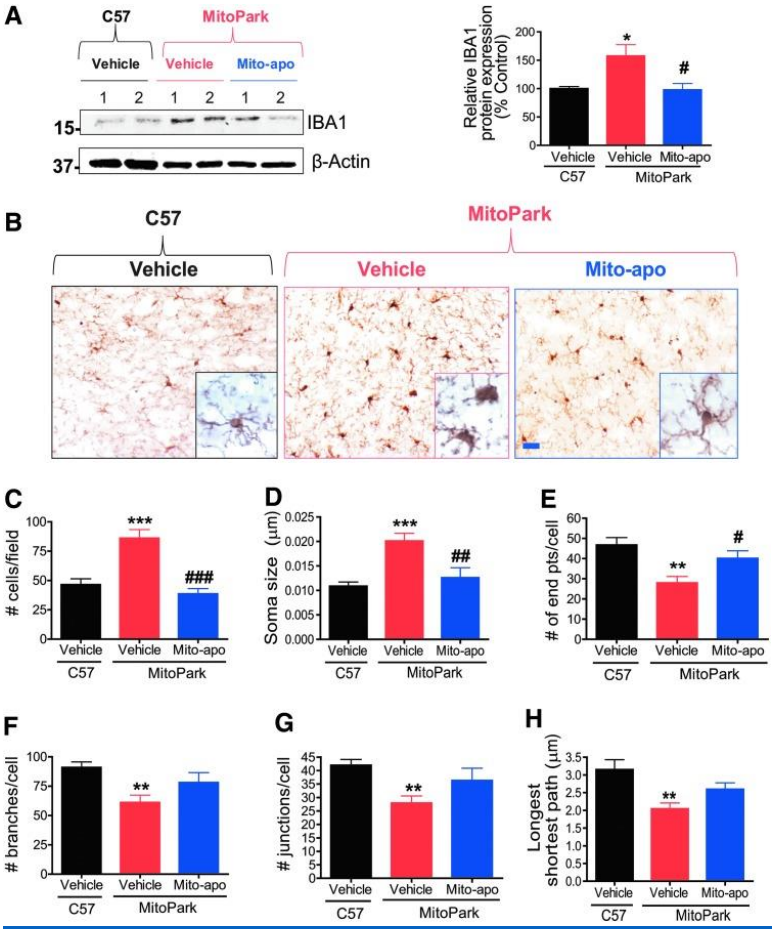

FIG. 5. Mito-apo inhibits microglia activation in the SN of MP mice. (A) Western blot and densitometric analysis of IBA1 protein in the SN (*n* = 6/group). **(B)** IBA1 DAB immunostained sections from 24-week mouse SN of vehicle-treated C57 (*left*), vehicle-treated MP (*middle*), and Mito-apo-treated MP mice (*right*) showing microglia morphology (scale bar = 200 µm). ImageJ analysis of microglia for cells per field **(C)**, soma size **(D)**, number of endpoints per cell **(E)**, number of branches per cell **(F)**, number of junctions per cell **(G)**, and longest-shortest path **(H)**. Graphical results represented as the mean ± SEM (*n* = 5–7 mice/group). **p* < 0.05 *versus* C57 control; ***p* < 0.01, ****p* < 0.001 *versus* vehicle-treated C57; $^{\#}p$ < 0.05 *versus* vehicle-treated MP; $^{\#\#}p$ < 0.01 *versus* vehicle-treated MP; $^{\#\#\#}p$ < 0.001 *versus* vehicle-treated MP. See also Supplementary Figure S5.

Mito-apo decreases NOX2 and iNOS activity in microglia

An increase in NOX2 and iNOS expression during microglial activation may synergistically contribute to neuronal death (46). Since Mito-apo treatment inhibits microglia activation, we then tested whether it also dampened NOX2 activity and iNOS induction. Immortalized microglial cells were generated as described in the Materials and Methods section and obtained as a kind gift from Dr. Douglas Golenbock for conducting the following experiments (37). To better define the therapeutic target of Mito-apo in microglia, we examined NOX2 activation by $p47^{phox}$ translocation from cytosol to the membrane. Western blot analysis revealed that lipopolysaccharide (LPS) robustly increased the amount of membrane-bound $p47^{phox}$ in microglia, while the cytosolic $p47^{phox}$ was significantly reduced when compared to control cells (Fig. 6A). Furthermore, this is substantiated by immunocytochemical results showing increased colocalization of $p47^{phox}$ with cholera toxin subunit B (CTXB-555), a membrane marker, following LPS treatment (Fig. 6B). LPS-stimulated microglia cotreated with Mito-apo showed a significant decrease in membrane $p47^{phox}$ and an increase in cytosolic $p47^{phox}$ when compared to vehicle-treated LPS-stimulated microglia (Fig. 6A). Similarly, reduced colocalization of $p47^{phox}$ and

CTXB-555 was observed in Mito-apo-treated LPS-stimulated microglia (Fig. 6B). Together, these data suggest that Mito-apo can effectively prevent p47^{phox} membrane recruitment, which is otherwise obligatory for NOX2 activation.

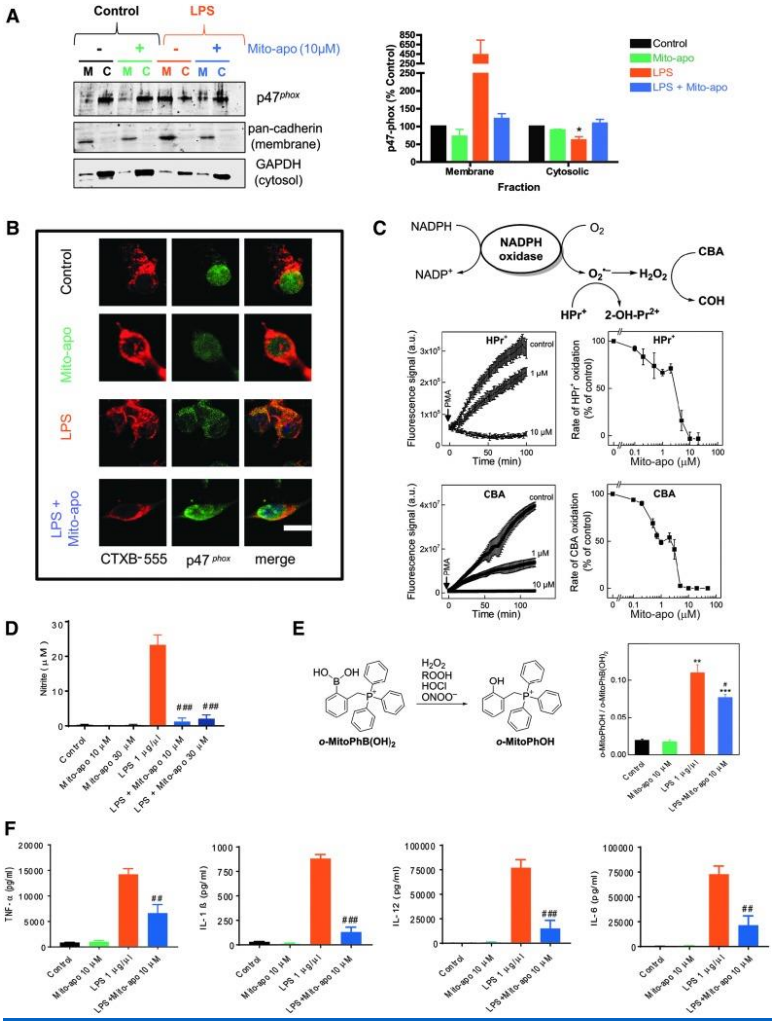

FIG. 6. Mito-apo decreases NOX2 and iNOS activity in microglia. (A) Western blot and accompanying densitometric analysis of membrane and cytosolic fractions from control and LPS-stimulated microglia treated with or without 10 μM Mito-apo. **(B)** Immunocytochemistry revealing increased membrane colocalization of p47^{phox} upon LPS stimulation that is reduced with Mito-apo treatment. CTXB = cholera toxin subunit B with 555 fluorophore. **(C)** ATRA-differentiated HL60 cells were pretreated with Mito-apo for 30 min in HBSS supplemented with HEPES buffer (25 mM, pH 7.4) and DTPA (0.1 mM), followed by the addition of the probe and PMA (1 μM). The slope of the fluorescence intensity monitored over 2 h was used to measure the probe oxidation rate. **(D)** Nitric oxide production from microglia as estimated in supernatant by Griess assay of nitrite levels. **(E)** LPS-induced oxidation of *o*-MitoPhB(OH)$_2$ to *o*-MitoPhOH in microglia was inhibited by Mito-apo. **(F)** Luminex multiplex assay showing levels of TNF-α, IL-1β, IL-6, and IL-12 in supernatant from LPS-stimulated microglia (*n* = 4–6/group). Graphical results represented as the mean ± SEM (*n* = 3/group). $^{*}p < 0.05$ *versus* C57 control. $^{**}p < 0.01$, $^{***}p < 0.001$ *versus* control; $^{\#}p < 0.05$, $^{\#\#}p < 0.01$, $^{\#\#\#}p < 0.001$ *versus* LPS. See also Supplementary Figure S7. ATRA, all-trans retinoic acid; IL, interleukin; LPS, lipopolysaccharide; PMA, phorbol myristate acetate; TNF-α, tumor necrosis factor α.

Our previous publication shows that HL60 cells differentiated into neutrophils and treated with phorbol myristate acetate (PMA) can be used as a reliable source of endogenous NOX2 activation (73). To test the effect of Mito-apo treatment on NOX2 activity in intact cells, we used all-trans retinoic acid (ATRA)-differentiated HL60 cells, stimulated with PMA. We utilized hydropropidine (HPr^+) as the probe for NOX2-derived superoxide radical anion ($O_2^{\bullet-}$) and coumarin boronic acid (CBA) as a probe for hydrogen peroxide (H_2O_2) (73, 75). The 30-min pretreatment of cells with a low micromolar concentration (<10 µM) of Mito-apo led to a dose-dependent inhibition of the PMA-stimulated generation of $O_2^{\bullet-}$ and H_2O_2 (Fig. 6C). This demonstrates that Mito-apo directly or indirectly mitigates NOX2 activity.

Next, we tested the effect of Mito-apo on oxidant production in microglial cells. After exposing microglial cells to LPS (1 µg/ml) for 12 h in the presence or absence of Mito-apo (10–30 µM), Griess assay revealed that Mito-apo completely blocked LPS-induced nitric oxide production (Fig. 6D). In addition, LC-MS-based monitoring of the conversion of the *o*-MitoPhB$(OH)_2$ probe into the phenolic product (*o*-MitoPhOH) (10, 11, 74, 75) indicates significant suppression of mitochondrial oxidant levels (Fig. 6E). The Mito-apo cotreatment also significantly attenuated LPS-induced increases in the levels of supernatant cytokines, including tumor necrosis factor α (TNF-α), interleukin-1β (IL-1β), IL-12, and IL-6, as measured by Luminex multiplex immunoassay (Fig. 6F). For comparison, 10 µM vitamin C and 10 µM apocynin were also tested, but neither treatment significantly attenuated LPS-stimulated neuroinflammation endpoints at this dose (Supplementary Fig. S6).

Mito-apo attenuates iNOS and NOX2 expression in the SN of MitoPark mice

Consistent with our *in vitro* results, double immunolabeling experiments confirmed that the increased iNOS expression occurred in $IBA1^+$ microglia and was significantly reduced in Mito-apo-treated MitoPark mice (Fig. 7A). Western blotting revealed an increase in iNOS expression in the SN of 24-week MitoPark mice that was significantly attenuated in the Mito-apo-treated mice (Fig. 7B). In addition, $gp91^{phox}$, a subunit of NOX2, was upregulated in microglia of the SN of aged MitoPark mice (Fig. 7C, D), yet was significantly reduced in the Mito-apo-treated group, as evidenced by Western blotting and IHC double labeling with IBA1.

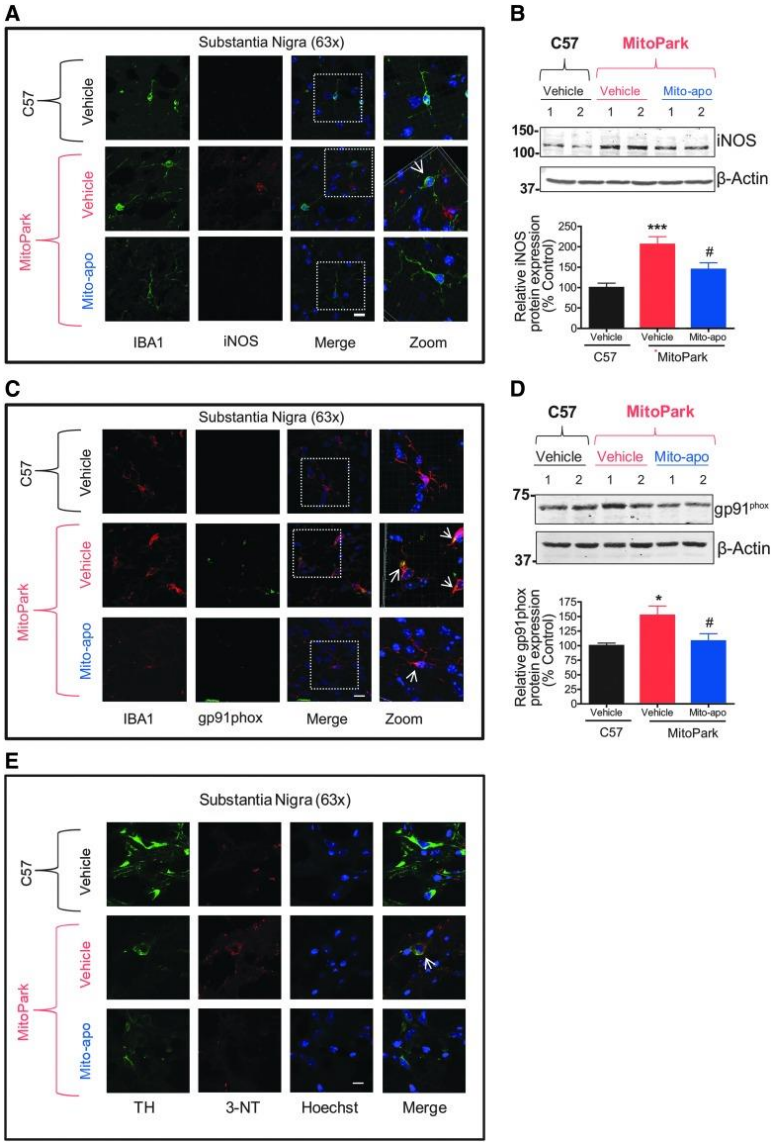

FIG. 7. Mito-apo inhibits iNOS and NOX2 expression in the SN of MP mice. Determination of NOX2 and iNOS activity in the SN. **(A)** Twenty-four-week mouse tissues of vehicle-treated C57 (*top*), vehicle-treated MP (*middle*), and Mito-apo-treated MP mice (*bottom*) stained for IBA1 and iNOS (scale bar = 10 μm). Merged MP image shows colocalization (*arrow*) of IBA1 and iNOS in SN tissues. **(B)** Representative Western blot and densitometric analysis of iNOS protein in the SN (n = 6/group). **(C)** IHC for IBA1 and gp91^{phox} of vehicle-treated C57 (*top*), vehicle-treated MP (*middle*), and Mito-apo-treated MP mice (*bottom*). Merged MP image shows colocalization (*arrows*) of IBA1 and gp91^{phox} in SN tissues. **(D)** Representative Western blot and densitometric analysis of gp91^{phox} protein in the SN (n = 6/group). **(E)** IHC for TH and 3-nitrotyrosine of vehicle-treated C57 (*top*), vehicle-treated MP (*middle*), and Mito-apo-treated MP mice (*bottom*). Graphical results represented as the mean ± SEM. $^{\#}p < 0.05$ *versus* vehicle-treated MP; $^{*}p < 0.05$ *versus* vehicle-treated C57; $^{***}p < 0.001$ *versus* vehicle-treated C57; IHC, immunohistochemistry.

Given that the NOX4 isoform has been shown to localize in the mitochondria of neurons (7), we also assessed whether Mito-apo alters NOX4 in our mitochondrially defective cell and animal models of PD. In TFAM-KD N27 dopaminergic cells, NOX4 levels increased significantly when compared to control cells (Supplementary Fig. S7A). However, Mito-apo treatment did not alter NOX4 levels in TFAM-KD cells. Furthermore, NOX4 mRNA and protein levels were not altered in the SN of either MitoPark mice or MitoParks treated with Mito-apo when

compared to age-matched control mice (Supplementary Fig. S7B, C). These data suggest that Mito-apo is more selective for NOX2 over NOX4 in neuronal cells and NOX4 is not a major contributor to oxidative damage in the MitoPark model.

Peroxynitrite, formed when superoxide reacts with nitric oxide, nitrates tyrosine residues on proteins and contributes to neuronal cell death (33, 75). Increased nitrative modification was evidenced by higher 3-NT expression in the SN of 24-week MitoPark mice compared to C57 black mice (Fig. 7E). Notably, 3-NT expression was significantly suppressed in Mito-apo-treated MitoPark mice. Overall, these data show that Mito-apo attenuated microglia activation and neuronal cell death in MitoPark mice by suppressing oxidative and nitrative stress.

Mito-apo is central nervous system bioavailable without systemic adverse effects

Finally, we determined if Mito-apo reaches its target brain tissues, the SN and striatum. Mice were orally administered Mito-apo (10 mg/kg), sacrificed, and tissues were harvested at 30 min, 3, 6, 12, 24, and 48 h. Striatal and nigral regions were processed for HPLC. Here, we have provided evidence that Mito-apo reaches its target brain tissues, the SN and striatum, and did not cause systemic adverse effects (Supplementary Fig. S8 and Tables 1 and and2).2). LC MS/MS analysis did not detect the Mito-apo in extra-nigral tissues. We also conducted a dose–response study at the 6-h time point, when Mito-apo availability peaks in brain tissues (Supplementary Fig. S8), yet did not detect any significant difference between 10 and 30 mg/kg Mito-apo oral administration.

Table 1. clinical pathology results for mice (*n* = 3) 3 hour postoral gavage with 10 mg/kg mito-apo-c_{11} using the abaxis system

			3-h Control				***3-h Mito-apo-C_{11}***			
Parameter	***Units***	**p**	***Mean***	***Min***	***Max***	***SD***	***Mean***	***Min***	***Max***	***SD***
Albumin	g/dl	0.31	3.23	2.40	3.90	0.62	3.77	3.50	4.00	0.21
Alkaline phosphatase	IU/L	1.00	70.67	56.00	88.00	13.20	70.67	63.00	81.00	7.59
ALT	IU/L	0.41	65.67	38.00	84.00	19.91	94.00	54.00	146.00	38.51
Amylase	U/L	0.38	1061.33	927.00	1316.00	180.17	1699.00	1050.00	2977.00	903.72
Total bilirubin	U/L	0.37	0.30	0.30	0.30	0.00	0.33	0.30	0.40	0.05
BUN	mg/dl	0.83	15.33	12.00	21.00	4.03	14.67	13.00	16.00	1.25
Calcium	mg/dl	0.50	11.73	11.50	12.20	0.33	11.50	11.20	11.90	0.29
Phosphorous	mg/dl	0.94	10.20	8.50	12.20	1.53	10.30	9.50	11.80	1.06
Creatinine	mg/dl	0.37	0.27	<0.20	0.40	0.09	0.20	<0.20	<0.20	0.00
Glucose	mg/dl	0.05	292.33	274.00	317.00	18.12	336.67	320.00	352.00	13.10
Sodium	mEq/L	0.84	159.00	156.00	161.00	2.16	159.33	159.00	160.00	0.47
Potassium	mEq/L	1.00	8.50	>8.50	>8.50	0.00	8.50	>8.50	>8.50	0.00
Total protein	g/dl	0.81	5.50	5.40	5.60	0.08	5.53	5.30	5.70	0.17

Table 2. clinical pathology results for mice (*n* = 3) 48 hour postoral gavage with 10 mg/kg mito-apo-c_{11}

			48-h Control				***48-h Mito-apo-C_{11}***			
Parameter	***Units***	**p**	***Mean***	***Min***	***Max***	***SD***	***Mean***	***Min***	***Max***	***SD***
Albumin	g/dl	0.23	4.07	3.70	4.40	0.29	4.37	4.30	4.50	0.09
Alkaline phosphatase	IU/L	0.02	134.00	119.00	159.00	17.80	82.00	72.00	91.00	7.79
ALT	IU/L	0.20	60.33	45.00	77.00	13.10	90.33	58.00	118.00	24.72
Amylase	U/L	0.05	858.33	816.00	935.00	54.31	1024.00	962.00	1118.00	67.59
Total bilirubin	U/L	0.52	0.37	0.30	0.40	0.05	0.33	0.30	0.40	0.05
BUN	mg/dl	0.15	14.67	13.00	18.00	2.36	17.67	17.00	18.00	0.47
Calcium	mg/dl	0.02	10.73	10.50	11.00	0.21	11.40	11.20	11.60	0.16
Phosphorous	mg/dl	0.01	8.30	8.10	8.50	0.16	10.03	9.40	10.40	0.45
Creatinine	mg/dl	1.00	0.20	0.20	0.20	0.00	0.20	0.20	0.20	0.00
Glucose	mg/dl	0.06	227.67	196.00	250.00	23.01	271.67	261.00	282.00	8.58
Sodium	mEq/L	0.14	159.00	156.00	161.00	2.16	162.00	161.00	163.00	0.82
Potassium	mEq/L	0.37	8.40	8.20	8.50	0.14	8.50	8.50	8.50	0.00

Total protein	g/dl	0.12	5.17	4.90	5.50	0.25	5.53	5.40	5.60	0.09

Clinical pathology can be particularly useful in predicting toxicity in animal models for preclinical evaluation (5, 59). Blood plasma, collected by cardiac puncture at 3 and 48 h after gavaging mice with 10 mg/kg Mito-apo, was analyzed using the Abaxis system. Clinical pathology variables are reported in Tables 1 and and2.2. At 3 h, the only significant difference between vehicle and Mito-apo-treated C57 black mice was blood glucose level (Table 1). As mice were not fasted, the range of values for both groups is considered acceptable (57). Alkaline phosphatase (ALP) levels, an indicator of hepatobiliary or bone disease, were significantly less in Mito-apo-treated mice than in controls after 48 h (Table 2), but still within normal reference intervals. Calcium and phosphorous levels were elevated in the Mito-apo-treated group, but no other significant changes were observed at 48 h postgavage. These results suggest that Mito-apo can rapidly cross the blood–brain barrier and persist in the central nervous system (CNS) to produce its neuroprotective effect without contributing to any major acute adverse effects.

Discussion

Oxidative stress, mitochondrial dysfunction, and neuroinflammation contribute to dopaminergic degeneration in PD (3, 13, 66). Reactive oxygen species (ROS) derived from NOX2 and mitochondria potentiate neurodegeneration through oxidative stress and promote proinflammatory events (12, 56). In this study, we tested a recently created pharmacophore, Mito-apo, in cell culture and animal models of mitochondrial dysfunction and neuroinflammation. First, Mito-apo treatment increased OCR in a dopaminergic cell line, indicating a bioenergetic effect. This was further clarified by showing that treatment with Mito-apo increased aconitase activity and ATP levels, improved mitochondrial structural integrity, and decreased mitochondrial oxidants in TFAM-KD N27 cells. In MitoPark mice, Mito-apo treatment attenuated progressive motor deficits, striatal neurotransmitter depletion, and nigrostriatal degeneration, suggesting a neuroprotective property. Mito-apo treatment also prevented microglial activation, proinflammatory mediators, NOX2 and iNOS activation, and oxidative stress marker formation. Thus, our data demonstrate anti-inflammatory, antioxidant, and neuroprotective properties of a new apocynin derivative, Mito-apo, in MitoPark mice that possess pathological features of chronic dopaminergic neurodegeneration, including mitochondrial dysfunction, oxidative damage, and neuroinflammation.

Mitochondrial dysfunction can be found in toxin-based models, such as the MPTP and 6-OHDA treatment paradigms, and in genetic models, such as the LRRK2- and PINK1-based models (3, 16, 44, 62, 71). Wang *et al.* (69) demonstrated that TFAM inactivation results in respiratory chain deficiency and increased *in vivo* apoptosis, and proposed that the resulting loss of mitochondrial function has important therapeutic implications for human disease. Although the MitoPark model, with TFAM knocked out in the nigrostriatal pathway, does not mirror any specific genetic mutation associated with PD, both TFAM and mitochondrial DNA changes have been implicated in aging and PD (2, 29, 30, 54). Similarly, the TFAM-KD N27 dopaminergic cells generated using the CRISPR/Cas9 system manifested mitochondrial dysfunction as reduced *m*-aconitase activity and ATP levels, increased oxidant production, and altered mitochondrial morphology. Our results clearly indicate that Mito-apo restores functional mitochondria by increasing mitochondrial bioenergetics and inhibiting production of oxidants. Thus, treatment with an MTA can alleviate the loss of mitochondrial structural and functional integrity in a cell culture model of mitochondrial dysfunction.

We next determined if Mito-apo exerts its protective action on mitochondrial redox *in vivo*. To gain insights into any effect of Mito-apo on oxidative stress amelioration in MitoPark mice, we monitored the EPR signals due to mitochondrial aconitase iron–sulfur clusters in brain tissue at cryogenic temperatures. ROS-induced oxidation of the catalytically required $[4Fe–4S]^{2+}$ cluster inactivates the aconitase enzyme due to loss of the labile iron ion, forming the EPR detectable $[3Fe–4S]^{+}$ cluster. Mito-apo treatment significantly inhibited the development of the $[3Fe–4S]^{+}$ cluster EPR signal from mitochondrial aconitase in MitoPark mice. These results suggest that Mito-apo

treatment can effectively block *m*-aconitase inactivation in aged MitoPark mice. Advancing age is a main risk factor in neurodegenerative disease and is correlated with increased mitochondrial dysfunction and oxidative stress, leading to irreversible structural changes in proteins, lipids, and DNA (51, 65, 68). Here we found that levels of 4-HNE-modified proteins, an unsaturated aldehyde generated during lipid peroxidation and marker of oxidative damage, were significantly higher in the SN of 24-week MitoPark brains compared to age-matched C57 black controls, yet Mito-apo treatment significantly decreased these levels. Hence, oxidative stress associated with the inherent mitochondrial dysfunction in the MitoPark model can be reduced by long-term, low-dose treatment with Mito-apo.

In the CNS, microglial activation and the production of proinflammatory factors, including cytokines, ROS, and RNS, are hallmarks of inflammatory reactions. Our IHC and Western blot analyses revealed significantly increased IBA1 expression in the SN of 24-week MitoPark mice coupled with increased soma size and fewer processes, suggesting increased microglia activation in 24-week MitoPark mice. Mito-apo-treated MitoPark mice had significantly fewer $IBA1^{+}$ cells, decreased soma size, and increased branching complexity consistent with ramified microglia when compared to vehicle-treated MitoPark mice. Mito-apo treatment also effectively decreased iNOS and $gp91^{phox}$ protein levels in the $IBA1^{+}$ nigral cells of MitoPark mice. Activation of NOX2 and mitochondrial ROS signaling was proposed to involve crosstalk that increases production of both in a feed-forward cycle (15, 46). NOXs play an obvious role in dopaminergic neurodegeneration via ROS generation (9, 52). However, their involvement in PD is potentially more complex, involving other contributing factors such as protein aggregation and mitochondrial dysfunction (13, 15, 20). In animal models of PD in which proinflammatory enzymes are elevated, anti-inflammatory therapies have successfully modulated the neurodegenerative process (32, 56). Reactive microgliosis results from stressed neurons secreting factors that activate microglia, beginning the cycle of neuroinflammation and neuronal damage underlying neurodegenerative diseases (4, 42, 45). Although neuroinflammation was not originally defined in the MitoPark model, we show here that reactive microgliosis is likely involved, implicating an important therapeutic potential for MTA and anti-inflammatory drugs in PD. This finding is salient considering that chronic neuroinflammation is now perceived to mediate PD pathogenesis and current drugs only provide symptomatic relief (60, 66).

By restricting $p47^{phox}$ from translocating to the membrane and subsequently inhibiting superoxide production by NOX2 in microglia, Mito-apo reduced inflammation in addition to its role as an antioxidant in neurons. This combined effect on both microglia and neurons may help to break up a self-propelling cycle of neuroinflammation and neurodegeneration characteristic of PD. This approach was also recently found to be effective in the toxin-based MPTP model (28). It should be noted that the severity of the MitoPark model allowed for only a modest recovery of motor function with Mito-apo treatment due to the complex nature of the neurodegenerative process. We explored the potential benefit of a higher dose by performing a dose–response study at the time point with the highest concentration of Mito-apo in the brain (Supplementary Fig. S3D). However, our results did not show significantly more Mito-apo detectable in brain tissues of the 30 mg/kg group *versus* 10 mg/kg group. This suggests that even at a higher dose, Mito-apo would not have provided an additional benefit. Additional analysis of Mito-apo by LC-MS/MS did not detect the compound, but spiking the samples with 0.1 µM concentration detected the peak. A detailed pharmacokinetic analysis of Mito-apo is still warranted. Although oxidative stress and neuroinflammation are key players in the cell death mechanisms leading to PD, other mechanisms such as protein aggregation, ubiquitin–proteasome system dysfunction, mitophagy, and inflammasome-dependent neuroinflammation have not yet been fully addressed in this model or with this compound. Furthermore, our group and others have shown that targeting a single pathophysiological pathway is not typically enough to completely restore function in the MitoPark model (24, 41). These observations warrant future studies into the therapeutic role of Mito-apo and the development of combination therapy modalities for PD.

Recently, we have demonstrated that Mito-apo prevents hyposmia and motor deficits in the LRRK2 mouse model (19). However, the effect of Mito-apo on mitochondrial function, microglial activation, NOX2 activation, and dopaminergic degeneration was not directly investigated in that model. Although circadian and cognitive changes occur in MitoPark mice (25, 43), the nonmotor Parkinsonian phenotype of these mice still needs to be fully characterized. Moreover, Mito-apo efficacy in treating nonmotor symptoms in PD animal models should be evaluated since antioxidants have been shown to successfully improve cognitive and neuropsychiatric symptoms in various neurodegenerative models (64, 67).

Based on our findings using a progressively degenerating and mitochondrially dysfunctional animal model of PD, Mito-apo may outperform other experimental drugs by being well tolerated yet bioavailable in the brain when delivered orally, and by exhibiting potent antineuroinflammatory and antioxidant effects at a low dose. Here we have demonstrated that Mito-apo protected dopaminergic neurons and reduced oxidative and nitrative stress, glial cell activation, and inflammatory reactions. NOX2-mediated superoxide production is thought to be essential for maintaining chronic neuroinflammation, which potentiates the neurodegenerative process through oxidative stress (9, 52). NOX2 knockout or treatment with NOX2 inhibitors in cell culture and mouse studies suggests that inhibiting NOX2 breaks the vicious, self-propelling cycle of reactive microgliosis, making it a valuable target for PD therapy (61, 70). These properties strongly support potential clinical applications for Mito-apo as a viable neuroprotective and antineuroinflammatory drug for treating PD when compared to conventional therapeutic approaches that only target downstream consequences of microglia activation and inflammation-mediated oxidative stress. Overall, we demonstrate that Mito-apo treatment effectively attenuates progressive motor deficits, neuroinflammation, neurochemical depletion, and loss of nigral TH neurons, revealing a neuroprotective effect in a comprehensive PD model that recapitulates salient features of chronic progressive dopaminergic neurodegeneration. Our proof-of-principle preclinical study warrants further translation of Mito-apo to preclinical safety evaluations and to subsequent clinical testing.

Materials and Methods

Chemicals

Rotenone (R8875), oligomycin (75351), antimycin A (A8674), dopamine hydrochloride (H8502), 3-4-dihydroxyphenylacetic acid (DOPAC, 850217), homovanillic acid (HVA, H1252), 3,3’-diaminobenzidine (DAB, D5637), Griess reagent (4410), puromycin (P8833), and hydrogen peroxide (H325) were all purchased from Sigma (St. Louis, MO). The CellTiter-Glo Cell Viability assay kit (G5421) was bought from Promega (Madison, WI). We purchased RPMI 1640 (11875093), Dulbecco's modified Eagle's medium (DMEM) (11330), fetal bovine serum (FBS, 26140), l-glutamine (25030081), penicillin–streptomycin (15140122), MitoTracker red (M-7512), and MitoSOX (M36008) from Invitrogen (Carlsbad, CA), and the Seahorse Flux Pak calibration solution and carbonilcyanide p-trifluoromethoxyphenylhydrazone (FCCP) (103015) from Seahorse Biosciences (Billerica, MA). The aconitase assay kit (ab83459), anti-4-HNE (mab3249), anti-IBA1 (ab5076), and gp91^{phox} (ab129068) antibodies were purchased from Abcam (Cambridge, MA). Anti-NOS2 (sc-650) and p47^{phox} (H-195) antibodies were obtained from Santa Cruz Biotech (Dallas, TX), anti-IBA1 antibody (019-19741) was purchased from Wako (Richmond, VA), and anti-TH (mab318) and anti-3-NT (06-284) antibodies were purchased from Millipore (Billerica, MA).

Mito-apocynin synthesis

Mito-apo-C2 and Mito-apo-C11 were synthesized as described previously (19). Briefly, acetylvanillic acid and thionyl chloride were mixed to form acetylvanillic acid chloride, which was dissolved in dichloromethane and amino alkyl triphenyl phosphonium bromide and pyridine. The solution was purified on a silica gel column and the acetyl group was removed by hydrolysis.

Cell culture and CRISPR/Cas-based knockout of TFAM in N27 cells

For *in vitro* mitochondrial function studies, the rat immortalized mesencephalic dopaminergic neuronal cell line ($1RB_3AN_{27}$ or N27) was cultured in RPMI 1640 containing 2 mM l-glutamine, 50 U of penicillin, and 50 µg/ml of streptomycin with 0–10% FBS in incubators at 37°C and 5% CO_2 as previously described by our laboratory (8).

The lentivirus-based CRISPR/Cas9 KO plasmid, pLV-U6gRNA-Ef1aPuroCas9GFP-TFAM, with the TFAM gRNA target sequence directed against the exon 1 sequence (CPR555e5e4099bf84.98), was purchased from Sigma-Aldrich. To make lentivirus, the lenti-CRISPR/Cas9 TFAM KO plasmid and control plasmid were transfected into 293FT cells using the Mission Lentiviral Packaging Mix (SHP001; Sigma-Aldrich) according to the manufacturer's instructions. The lentivirus was harvested 48 h post-transfection and titers were measured using the Lenti-X™ p24 Rapid Titer Kit (632200; Clontech, Mountain View, CA). For stable KD of TFAM in N27 cells, six-well plates containing 0.1×10^6/well had lentivirus added the following morning to the media at an MOI of 100. After 24 h, fresh media supplemented with puromycin (50 µg/ml) was added to the cells for stable cell selection.

The wild-type microglial cell line, obtained as a kind gift from Dr. Golenbock at the University of Massachusetts, was used for neuroinflammation experiments and cultured in DMEM containing 2 mM l-glutamine, 50 U of penicillin, and 50 µg/ml of streptomycin with 2% FBS in six-well plates at a density of 1.5×10^6/well. The cell line was immortalized from wild-type C57 mouse primary microglia by infection with J2 recombinant retrovirus microglia and has been characterized by Halle *et al.* (37).

Mitochondrial oxygen consumption

The Seahorse XF96 analyzer was used to monitor basal OCR in N27 dopaminergic neuronal cells at different stages as previously described (8). Briefly, after pre-equilibrating the cartridge containing the mito-stressors oligomycin (1 µg/ml), FCCP (1 µM), and antimycin A (10 µM) in injection ports, a plate with cells pretreated in serum-free media for 3 h with 0, 10, or 30 µM Mito-apo-C_2 and 1 µM rotenone was placed into the Seahorse analyzer. OCR readouts were measured in pmol/min.

Cell viability, aconitase, and NOX2 activity

The CellTiter-Glo Luminescent Cell Viability (used to measure intracellular ATP levels) and aconitase activity assays were performed as per the manufacturer's instructions using control and TFAM stable KD N27 cells or microglia. The CellTiter-Glo Luminescent Cell Viability assays were performed using control or TFAM stable KD N27 cells (0.8×10^4/well) in a white opaque-walled 96-well plate.

For the aconitase activity assay, 1×10^6 cells were plated in a T25 flask. After treatments, mitochondrial fractions were collected and lysed as per the manufacturer's instructions. Readings at 450 nm were obtained using a SpectraMax plate reader and normalized to protein concentrations determined by Bradford assay.

NADPH oxidase activity was determined in differentiated human acute promyelocytic leukemia (*d*HL60) cells, as recently reported (73, 75). Hydropropidine probe (20 µM), in the presence of DNA (0.1 mg/ml), was used to monitor superoxide production, while coumarin boronic acid (100 µM) was used to monitor H_2O_2 formation. HL60 cells were maintained and differentiated with ATRA (1 µM) for 5 days as described previously (73). The differentiated cells were pretreated with Mito-apo for 30 min in HBSS supplemented with HEPES buffer (25 mM, pH 7.4) and DTPA (0.1 mM), followed by the addition of the probe and PMA (1 µM). Immediately after addition of PMA, the plates were placed in the plate reader and fluorescence intensity monitored over 2 h. The slope of the fluorescence intensity over time was used to measure the probe oxidation rate. The rate of probe oxidation in samples treated with pure DMSO (0.1% vol/vol) was taken as 100%.

Oxidation of mitochondrial boronate probe

Mitochondria-targeted boronates were proposed for site-specific detection of mitochondrial H_2O_2 (10, 11). For adjusting the results for differential uptake/availability of the probe in mitochondria, the use of a ratio of the phenolic product to probe level was proposed (10, 11). The *o*-MitoPhB(OH)$_2$ probe (74, 75) was incubated with microglial cells (50 µM, 1 h) before collecting the cells. The samples were prepared and analyzed by LC-MS/MS using the deuterated analogs d_{15}-MitoPhB(OH)$_2$ and d_{15}-MitoPhOH as the internal standards, as described recently (74, 75).

MitoTracker and MitoSOX

N27 dopaminergic cells grown on poly-d-lysine-coated glass coverslips in 24-well plates were treated in 2% FBS media for 12 h with 0, 10, or 30 µM Mito-apo-C_2 or 1 µM rotenone, and then washed twice with PBS. CMXRos MitoTracker Red dye (working concentration of 200 nM) was incubated at 37°C for 12 min. ImageJ was used to quantify mitochondrial parameters as described previously (8, 14). MitoSOX reagent (working concentration of 5 µM) was used to detect mitochondrial oxidant(s) production in live N27 cells as per the manufacturer's instructions. It should be noted that MitoSOX fluorescence does not allow for identification of the specific type of oxidant(s) detected.

Nitric oxide and cytokine detection

Microglia were cotreated for 12 h with 1 µg/ml LPS and 0, 10, or 30 µM Mito-apo-C_{11}. Supernatant was used to determine extracellular cytokine levels using the Luminex bead-based immunoassay with recombinant standards for IL-6, IL-12, TNF-α, and IL-1β. Nitric oxide production was measured as media nitrite levels using Griess reagent and sodium nitrite standard curve as previously described (35).

Animals and treatments

MitoPark mice were a kind gift of Dr. Nils-Goran Larson at the Max Planck Institute for Biology and Ageing in Cologne, Germany. All mice for this study were bred and housed under standard conditions (*ad libitum food,* a 12-h light cycle, constant temperature and humidity) at the Iowa State University (ISU) as approved by the Institutional Animal Care and Use Committee. MitoPark and age-matched control mice were oral gavaged with either 10 mg/kg Mito-apo-C_{11} dissolved in 10% ethanol in PBS or an equivolume vehicle solution thrice weekly from age 13 to 24 weeks. Mice were subjected to behavioral testing, and neurochemical and histological measurements were performed at age 24 weeks.

Behavior

Open-field and rotarod experiments were performed as previously described (32). Briefly, open-field measurements of spontaneous locomotor activity were accomplished using VersaMax (monitor RXYZCM-16, analyzer VMAUSB; AccuScan, Columbus, OH) during a 10-min acquisition period following a 2-min accustomization. Coordination was assessed by rotarod (AccuScan) performance at 20 rpm for five trials not exceeding 20 min.

HPLC analysis of neurotransmitters

Striatal lysates were prepared in an antioxidant buffer containing 0.2 M perchloric acid, 0.1% $Na_2S_2O_5$, 0.05% NaEDTA, and isoproterenol as an internal standard as previously described (33). Samples were sonicated for 2 min, centrifuged for 10 min, and filtered through a 0.2 µm filter before running. Samples were placed into an autosampler (WPS-3000TSL; Thermo Scientific) at 4°C and separated isocratically by a reversed-phase C18 column at 0.6 ml/min (pump, Ultimate 3000 ISO-3100SD). Electrochemical detection (CoulArray 5600A) was performed using potentials of 350, 0, −150, and 220 mV (microdialysis cell 5014B, guard cell 5020) to detect

dopamine, DOPAC, and HVA. Chromatograph integration and analyses were performed using Chromeleon (7.1.3) and ESA CoulArray (3.10) software.

Western blotting

Western blot lysates from the striatum and SN were prepared in RIPA buffer with protease and phosphatase inhibitors (Pierce Biotechnology) and run on a 10–15% sodium dodecyl sulfate/polyacrylamide gel electrophoresis (SDS-PAGE) as previously described (33). Following SDS-PAGE electrophoresis, proteins were transferred to a nitrocellulose membrane (Bio-Rad). After blocking for 1 h in LiCor blocking buffer or milk, primary antibodies including 4-HNE (1:2000), TH (1:1500), iNOS (1:500), IBA1 (1:1200), and β-actin (1:7000) were incubated at 4°C overnight. Secondary antibodies (Alexa Fluor 680 and Rockland IR800) were incubated at RT for 1 h and images were captured via LiCor Odyssey imager. Densitometric analysis was done using ImageJ software.

IHC and confocal imaging

Perfusion, sectioning, and IHC were performed as previously described by Ghosh *et al.* (33). Animals were transcardially perfused with PBS and 4% PFA. The next day, brains were cryoprotected with 30% sucrose and brain blocks were made in OCT. Cryo-solution containing ethylene glycol and sucrose was used to store 30-µm sections until use. Following washing, antigen retrieval was achieved by keeping sections at 80°C for 30 min in sodium citrate. Sections were incubated with primary antibodies overnight at 4°C. Appropriate secondary antibodies (Alexa Fluor 488 and 555) were incubated with sections for 1.5 h, followed by 7 min with Hoechst stain. Dehydrated slides were mounted using DPX.

Images (20–30 ×) were captured with an inverted microscope attached to a SPOT digital camera. For confocal imaging, the ISU Microscopy Facility's Leica DMIRE2 confocal microscope was used to acquire 63 × z-stack images, which were converted to maximum projection images using Imaris software.

DAB immunostaining and cell counting

For DAB staining, IHC was performed on 30-µm SN sections. A biotinylated secondary antibody followed by incubation with an avidin peroxidase solution (Vector labs) was used to yield a brown stain after incubation with DAB solution. Stereological counting of TH^+ neurons was done on every sixth section at 40 × using Stereo Investigator software (MicroBrightField) with an optical fractionator. Images (20 ×) for $IBA1^+$ microglia analysis were acquired with Spot software. ImageJ software was used to count microglial cells, adjust threshold, convert images to binary, skeletonize, and analyze skeleton (49).

Electron paramagnetic resonance

EPR spectra were recorded on a Bruker ELEXSYS E600 spectrometer equipped with a Super-X microwave bridge with an integrated microwave counter, an ER4112SHQ resonant cavity operating at 9.38 GHz, and an Oxford Instruments ESR900 helium flow cryostat with an ITC503 temperature controller. Spectra were recorded at 12 K with 5 mW microwave power and 10 G magnetic field modulation at 100 kHz; this modulation amplitude determined the spectral resolution. Scans of 4096 points, an 8000 G field envelope, and a 3-min duration were averaged over 60–180 min to provide the final spectrum. A background spectrum collected on frozen water was subtracted from experimental spectra. Contributions of each of the paramagnetic centers of the mitochondrial proteins to the experimental spectra were estimated by fitting a library of computed spectra corresponding to the mitochondrial respiratory chain centers and the [3Fe–4S] cluster of aconitase, using a Levenberg–Marquardt algorithm to minimize χ^2 (IGOR Pro v. 6.32A; Wavemetrics, Lake Oswego, OR). The contributions of each component were constrained to ≥0. Computed spectra of the individual components were calculated, using spin Hamiltonian parameters from the literature (23, 26, 36, 40, 50, 58, 72), with XSophe [Bruker Biospin; (38)].

Detection of Mito-apo-C11 in brain and blood

Mice were administered 10 mg/kg Mito-apo-C11 by oral gavage and then sacrificed at 30 min, 3, 6, 12, 24, or 48 h (*n* = 3/time point). Blood was collected by cardiac puncture into heparinized tubes for plasma, and various brain regions were dissected out and stored at −80°C. Tissue homogenates were then made using antioxidant buffer, as described above for neurotransmitter extraction. The standards prepared and used for quantification were 0.1, 0.3, 1.0, 10, and 30 μg. Samples were centrifuged and 0.2-μm filtered before analysis on an Agilent Technologies 1200 Series HPLC system using a 20 -μl injection volume. Separation was performed with a Kinetex C18 column, operated at a flow rate of 1.5 ml/min and a temperature of 40°C, using a gradient elution (solvent A = 90% water, 10% acetonitrile, solvent B = 100% acetonitrile) over 10 min. Mito-apo-C11 was quantified by UV absorbance (collected at wavelengths of 262 and 292 nm) with an average retention time of 6.35 min. Standards were fit to a linear regression and data were analyzed using GraphPad Prism 4.0.

Statistical analysis

Data were analyzed by one-way analysis of variance with Bonferroni post-test using Prism 4.0 software. Differences with *p*-values ≤0.05 were considered significant.

Supplementary Material

Supplemental data:

Click here to view.(899K, zip)

Go to:

Abbreviations Used

4-HNE	4-hydroxynonenal
6-OHDA	6-hydroxydopamine
ALP	alkaline phosphatase
ATRA	all-trans retinoic acid
CBA	coumarin boronic acid
CNS	central nervous system
CRISPR	clustered regularly interspaced short palindromic repeats
DA	dopamine
DMEM	Dulbecco's modified Eagle's medium
l-DOPA	l-3,4-dihydroxyphenylalanine
DOPAC	3,4-dihydroxyphenylacetic acid
EPR	electron paramagnetic resonance
FBS	fetal bovine serum
FCCP	carbonilcyanide p-trifluoromethoxyphenylhydrazone
HPLC	high-performance liquid chromatography
HPr^+	hydropropidine
HVA	homovanillic acid
IBA1	ionized calcium-binding adapter molecule 1
iNOS	inducible nitric oxide synthase
IL	interleukin
KD	knockdown
LPS	lipopolysaccharide

LRRK2	leucine-rich repeat kinase 2
Mito-apo	Mito-apocynin
MP	MitoPark
MPTP	1-methyl-4-phenyl-1,2,3,6-tetrahydropyridine
MTA	mitochondria-targeted antioxidants
NOX	NADPH oxidase
OCR	oxygen consumption rate
PD	Parkinson's disease
PINK1	PTEN-induced putative kinase 1
PMA	phorbol myristate acetate
ROS	reactive oxygen species
SN	substantia nigra
TFAM	mitochondrial transcription factor A
TH	tyrosine hydroxylase
TNFα	Tumor necrosis factor α

Acknowledgments

This study was funded by NIH grants R01 NS039958 (to B.K. and A.K.), NS074443 (to A.K.), the NIH/NIBIB National Biomedical EPR Center (P41 EB001980), U.S. Army Medical Research and Materiel Command (Grant No. W81XWH-11-1-0700), by the Henry R. and Angeline E. Quadracci Chair Endowment (B.K.), and the Eugene and Linda Lloyd Chair Endowment (A.K.). We also thank Mrs. Monika Zielonka (Medical College of Wisconsin) for help in NOX2 activity assays and Gary Zenitsky (Iowa State University) for his assistance in the preparation of this article.

Authors' Contributions

A.G.K., M.L, and A.G. conceived and designed the experiments. M.L., A.G., A.C., J. Z., B.S., B.B., T.B., and S.S. performed the experiments. M.L., A.G., J. Z., B.B., T.B., and B.N. analyzed the data. M.A., J.L., S.G., D.K. contributed reagents, cell lines, and mouse strains. M.L., H.J, and V.A. wrote the article. A.G.K., A.K., and B.K. led the investigation, conceived the project, and wrote the article. All authors reviewed and edited the article.

Author Disclosure Statement

A.G.K. and B.K. hold a patent entitled “Neuroprotective Compounds and Their Use” for the Mito-apocynin treatment of Parkinson's disease. A.G.K. and V.A. are shareholders of PK Biosciences. The other authors have no conflicts of interest.

References

1. Anantharam V, Kaul S, Song C, Kanthasamy A, and Kanthasamy AG. Pharmacological inhibition of neuronal NADPH oxidase protects against 1-methyl-4-phenylpyridinium (MPP+)-induced oxidative stress and apoptosis in mesencephalic dopaminergic neuronal cells. Neurotoxicology 28: 988–997, 2007
2. Belin AC, Bjork BF, Westerlund M, Galter D, Sydow O, Lind C, Pernold K, Rosvall L, Hakansson A, Winblad B, Nissbrandt H, Graff C, and Olson L. Association study of two genetic variants in mitochondrial transcription factor A (TFAM) in Alzheimer's and Parkinson's disease. Neurosci Lett 420: 257–262, 2007
3. Blesa J. and Przedborski S. Parkinson's disease: animal models and dopaminergic cell vulnerability. Front Neuroanat 8: 155, 2014

4. Block ML. and Hong JS. Chronic microglial activation and progressive dopaminergic neurotoxicity. Biochem Soc Trans 35: 1127–1132, 2007
5. Boone L, Meyer D, Cusick P, Ennulat D, Bolliger AP, Everds N, Meador V, Elliott G, Honor D, Bounous D, and Jordan H. Selection and interpretation of clinical pathology indicators of hepatic injury in preclinical studies. Vet Clin Pathol 34: 182–188, 2005
6. Bove J. and Perier C. Neurotoxin-based models of Parkinson's disease. Neuroscience 211: 51–76, 2012
7. Case AJ, Li S, Basu U, Tian J, and Zimmerman MC. Mitochondrial-localized NADPH oxidase 4 is a source of superoxide in angiotensin II-stimulated neurons. Am J Physiol Heart Circ Physiol 305: H19–H28, 2013
8. Charli A, Jin H, Anantharam V, Kanthasamy A, and Kanthasamy AG. Alterations in mitochondrial dynamics induced by tebufenpyrad and pyridaben in a dopaminergic neuronal cell culture model. Neurotoxicology 53: 302–313, 2016
9. Chen SH, Oyarzabal EA, and Hong JS. Critical role of the Mac1/NOX2 pathway in mediating reactive microgliosis-generated chronic neuroinflammation and progressive neurodegeneration. Curr Opin Pharmacol 26: 54–60, 2016
10. Cochemé HM, Logan A, Prime TA, Abakumova I, Quin C, McQuaker SJ, Patel JV, Fearnley IM, James AM, Porteous CM, Smith RAJ, Hartley RC, Partridge L, and Murphy MP. Using the mitochondria-targeted ratiometric mass spectrometry probe MitoB to measure H2O2 in living Drosophila. Nat Protoc 7: 946–958, 2012
11. Cochemé HM, Quin C, McQuaker SJ, Cabreiro F, Logan A, Prime TA, Abakumova I, Patel JV, Fearnley IM, James AM, Porteous CM, Smith RAJ, Saeed S, Carré JE, Singer M, Gems D, Hartley RC, Partridge L, and Murphy MP. Measurement of H2O2 within living drosophila during aging using a ratiometric mass spectrometry probe targeted to the mitochondrial matrix. Cell Metab 13: 340–350, 2011
12. Cristovao AC, Choi DH, Baltazar G, Beal MF, and Kim YS. The role of NADPH oxidase 1-derived reactive oxygen species in paraquat-mediated dopaminergic cell death. Antioxid Redox Signal 11: 2105–2118, 2009
13. Cristovao AC, Guhathakurta S, Bok E, Je G, Yoo SD, Choi DH, and Kim YS. NADPH oxidase 1 mediates alpha-synucleinopathy in Parkinson's disease. J Neurosci 32: 14465–14477, 2012
14. Dagda RK, Cherra SJ, 3rd, Kulich SM, Tandon A, Park D, and Chu CT. Loss of PINK1 function promotes mitophagy through effects on oxidative stress and mitochondrial fission. J Biol Chem 284: 13843–13855, 2009
15. Dikalov S. Cross talk between mitochondria and NADPH oxidases. Free Radic Biol Med 51: 1289–1301, 2011
16. Dodson MW. and Guo M. Pink1, Parkin, DJ-1 and mitochondrial dysfunction in Parkinson's disease. Curr Opin Neurobiol 17: 331–337, 2007
17. Dohi K, Ohtaki H, Nakamachi T, Yofu S, Satoh K, Miyamoto K, Song D, Tsunawaki S, Shioda S, and Aruga T. Gp91phox (NOX2) in classically activated microglia exacerbates traumatic brain injury. J Neuroinflammation 7: 41, 2010
18. Dranka BP, Gifford A, Ghosh A, Zielonka J, Joseph J, Kanthasamy AG, and Kalyanaraman B. Diapocynin prevents early Parkinson's disease symptoms in the leucine-rich repeat kinase 2 (LRRK2R(1)(4)(4)(1)G) transgenic mouse. Neurosci Lett 549: 57–62, 2013
19. Dranka BP, Gifford A, McAllister D, Zielonka J, Joseph J, O'Hara CL, Stucky CL, Kanthasamy AG, and Kalyanaraman B. A novel mitochondrially-targeted apocynin derivative prevents hyposmia and loss of motor function in the leucine-rich repeat kinase 2 (LRRK2(R1441G)) transgenic mouse model of Parkinson's disease. Neurosci Lett 583: 159–164, 2014
20. Dranka BP, Zielonka J, Kanthasamy AG, and Kalyanaraman B. Alterations in bioenergetic function induced by Parkinson's disease mimetic compounds: lack of correlation with superoxide generation. J Neurochem 122: 941–951, 2012

21. Duty S. and Jenner P. Animal models of Parkinson's disease: a source of novel treatments and clues to the cause of the disease. Br J Pharmacol 164: 1357–1391, 2011
22. Ekstrand MI, Terzioglu M, Galter D, Zhu S, Hofstetter C, Lindqvist E, Thams S, Bergstrand A, Hansson FS, Trifunovic A, Hoffer B, Cullheim S, Mohammed AH, Olson L, and Larsson NG. Progressive parkinsonism in mice with respiratory-chain-deficient dopamine neurons. Proc Natl Acad Sci U S A 104: 1325–1330, 2007
23. Fecke W, Sled VD, Ohnishi T, and Weiss H. Disruption of the gene encoding the NADH-binding subunit of NADH: ubiquinone oxidoreductase in Neurospora crassa. Formation of a partially assembled enzyme without FMN and the iron-sulphur cluster N-3. Eur J Biochem 220: 551–558, 1994
24. Fell MJ, Mirescu C, Basu K, Cheewatrakoolpong B, DeMong DE, Ellis JM, Hyde LA, Lin Y, Markgraf CG, Mei H, Miller M, Poulet FM, Scott JD, Smith MD, Yin Z, Zhou X, Parker EM, Kennedy ME, and Morrow JA. MLi-2, a potent, selective, and centrally active compound for exploring the therapeutic potential and safety of LRRK2 kinase inhibition. J Pharmacol Exp Ther 355: 397–409, 2015
25. Fifel K. and Cooper HM. Loss of dopamine disrupts circadian rhythms in a mouse model of Parkinson's disease. Neurobiol Dis 71: 359–369, 2014
26. Finel M, Majander AS, Tyynela J, De Jong AM, Albracht SP, and Wikstrom M. Isolation and characterisation of subcomplexes of the mitochondrial NADH:ubiquinone oxidoreductase (complex I). Eur J Biochem 226: 237–242, 1994
27. Galter D, Pernold K, Yoshitake T, Lindqvist E, Hoffer B, Kehr J, Larsson NG, and Olson L. MitoPark mice mirror the slow progression of key symptoms and L-DOPA response in Parkinson's disease. Genes Brain Behav 9: 173–181, 2010
28. Gao HM, Liu B, and Hong JS. Critical role for microglial NADPH oxidase in rotenone-induced degeneration of dopaminergic neurons. J Neurosci 23: 6181–6187, 2003
29. Gatt AP, Jones EL, Francis PT, Ballard C, and Bateman JM. Association of a polymorphism in mitochondrial transcription factor A (TFAM) with Parkinson's disease dementia but not dementia with Lewy bodies. Neurosci Lett 557 Pt B: 177–180, 2013
30. Gaweda-Walerych K, Safranow K, Maruszak A, Bialecka M, Klodowska-Duda G, Czyzewski K, Slawek J, Rudzinska M, Styczynska M, Opala G, Drozdzik M, Kurzawski M, Szczudlik A, Canter JA, Barcikowska M, and Zekanowski C. Mitochondrial transcription factor A variants and the risk of Parkinson's disease. Neurosci Lett 469: 24–29, 2010
31. Ghosh A, Chandran K, Kalivendi SV, Joseph J, Antholine WE, Hillard CJ, Kanthasamy A, Kanthasamy A, and Kalyanaraman B. Neuroprotection by a mitochondria-targeted drug in a Parkinson's disease model. Free Radic Biol Med 49: 1674–1684, 2010
32. Ghosh A, Kanthasamy A, Joseph J, Anantharam V, Srivastava P, Dranka BP, Kalyanaraman B, and Kanthasamy AG. Anti-inflammatory and neuroprotective effects of an orally active apocynin derivative in pre-clinical models of Parkinson's disease. J Neuroinflammation 9: 241, 2012
33. Ghosh A, Langley MR, Harischandra DS, Neal ML, Jin H, Anantharam V, Joseph J, Brenza T, Narasimhan B, Kanthasamy A, Kalyanaraman B, and Kanthasamy AG. Mitoapocynin treatment protects against neuroinflammation and dopaminergic neurodegeneration in a preclinical animal model of Parkinson's disease. J Neuroimmune Pharmacol 11: 259–278, 2016
34. Good CH, Hoffman AF, Hoffer BJ, Chefer VI, Shippenberg TS, Bäckman CM, Larsson N-G, Olson L, Gellhaar S, Galter D, and Lupica CR. Impaired nigrostriatal function precedes behavioral deficits in a genetic mitochondrial model of Parkinson's disease. FASEB J 25: 1333–1344, 2011
35. Gordon R, Hogan CE, Neal ML, Anantharam V, Kanthasamy AG, and Kanthasamy A. A simple magnetic separation method for high-yield isolation of pure primary microglia. J Neurosci Methods 194: 287–296, 2011

36. Haddy A. and Smith G. Transition metal and organic radical components of carp liver tissue observed by electron paramagnetic resonance spectroscopy. Comp Biochem Physiol Part B Biochem Mol Biol 123: 407–415, 1999
37. Halle A, Hornung V, Petzold GC, Stewart CR, Monks BG, Reinheckel T, Fitzgerald KA, Latz E, Moore KJ, and Golenbock DT. The NALP3 inflammasome is involved in the innate immune response to amyloid-[beta]. Nat Immunol 9: 857–865, 2008
38. Hanson GR, Gates KE, Noble CJ, Griffin M, Mitchell A, and Benson S. XSophe-Sophe-XeprView: A computer simulation suite (v.1.1.3) for the analysis of continuous wave EPR spectra. J Inorg Biochem 98: 903–916, 2004
39. Jin H, Kanthasamy A, Ghosh A, Anantharam V, Kalyanaraman B, and Kanthasamy AG. Mitochondria-targeted antioxidants for treatment of Parkinson's disease: preclinical and clinical outcomes. Biochim Biophys Acta 1842: 1282–1294, 2014
40. Kennedy MC, Antholine WE, and Beinert H. An EPR investigation of the products of the reaction of cytosolic and mitochondrial aconitases with nitric oxide. J Biol Chem 272: 20340–20347, 1997
41. Le Poul E, Bolea C, Girard F, Poli S, Charvin D, Campo B, Bortoli J, Bessif A, Luo B, Koser AJ, Hodge LM, Smith KM, DiLella AG, Liverton N, Hess F, Browne SE, and Reynolds IJ. A potent and selective metabotropic glutamate receptor 4 positive allosteric modulator improves movement in rodent models of Parkinson's disease. J Pharmacol Exp Ther 343: 167–177, 2012
42. Levesque S, Wilson B, Gregoria V, Thorpe LB, Dallas S, Polikov VS, Hong JS, and Block ML. Reactive microgliosis: extracellular micro-calpain and microglia-mediated dopaminergic neurotoxicity. Brain 133: 808–821, 2010
43. Li X, Redus L, Chen C, Martinez PA, Strong R, Li S, and O'Connor JC. Cognitive dysfunction precedes the onset of motor symptoms in the MitoPark mouse model of Parkinson's disease. PLoS One 8: e71341, 2013
44. Lin MK. and Farrer MJ. Genetics and genomics of Parkinson's disease. Genome Med 6: 48, 2014
45. Lull ME. and Block ML. Microglial activation and chronic neurodegeneration. Neurotherapeutics 7: 354–365, 2010
46. Mander P. and Brown GC. Activation of microglial NADPH oxidase is synergistic with glial iNOS expression in inducing neuronal death: a dual-key mechanism of inflammatory neurodegeneration. J Neuroinflammation 2: 20, 2005
47. Martinez TN. and Greenamyre JT. Toxin models of mitochondrial dysfunction in Parkinson's disease. Antioxid Redox Signal 16: 920–934, 2012
48. Miyazaki T, Iwasawa M, Nakashima T, Mori S, Shigemoto K, Nakamura H, Katagiri H, Takayanagi H, and Tanaka S. Intracellular and extracellular ATP coordinately regulate the inverse correlation between osteoclast survival and bone resorption. J Biol Chem 287: 37808–37823, 2012
49. Morrison HW. and Filosa JA. A quantitative spatiotemporal analysis of microglia morphology during ischemic stroke and reperfusion. J Neuroinflammation 10: 4, 2013
50. Nakamaru-Ogiso E, Matsuno-Yagi A, Yoshikawa S, Yagi T, and Ohnishi T. Iron-sulfur cluster N5 is coordinated by an HXXXCXXCXXXXXC motif in the NuoG subunit of *Escherichia coli* NADH:quinone oxidoreductase (complex I). J Biol Chem 283: 25979–25987, 2008
51. Naoi M, Maruyama W, Shamoto-Nagai M, Yi H, Akao Y, and Tanaka M. Oxidative stress in mitochondria: decision to survival and death of neurons in neurodegenerative disorders. Mol Neurobiol 31: 81–93, 2005
52. Nayernia Z, Jaquet V, and Krause KH. New insights on NOX enzymes in the central nervous system. Antioxid Redox Signal 20: 2815–2837, 2014
53. Panicker N, Saminathan H, Jin H, Neal M, Harischandra DS, Gordon R, Kanthasamy K, Lawana V, Sarkar S, Luo J, Anantharam V, Kanthasamy AG, and Kanthasamy A. Fyn kinase regulates microglial

neuroinflammatory responses in cell culture and animal models of Parkinson's disease. J Neurosci 35: 10058–10077, 2015
54. Picca A, Pesce V, Fracasso F, Joseph AM, Leeuwenburgh C, and Lezza AM. Aging and calorie restriction oppositely affect mitochondrial biogenesis through TFAM binding at both origins of mitochondrial DNA replication in rat liver. PLoS One 8: e74644, 2013
55. Pissadaki EK. and Bolam JP. The energy cost of action potential propagation in dopamine neurons: clues to susceptibility in Parkinson's disease. Front Comput Neurosci 7: 13, 2013
56. Qin L, Liu Y, Hong JS, and Crews FT. NADPH oxidase and aging drive microglial activation, oxidative stress, and dopaminergic neurodegeneration following systemic LPS administration. Glia 61: 855–868, 2013
57. Rossmeisl M, Rim JS, Koza RA, and Kozak LP. Variation in type 2 diabetes-related traits in mouse strains susceptible to diet-induced obesity. Diabetes 52: 1958–1966, 2003
58. Salerno JC. and Leigh JS. Crystal field of atypical low-spin ferriheme complexes. J Am Chem Soc 106: 2156–2159, 1984
59. Schnell MA, Hardy C, Hawley M, Propert KJ, and Wilson JM. Effect of blood collection technique in mice on clinical pathology parameters. Hum Gene Ther 13: 155–161, 2002
60. Sharma N. and Nehru B. Characterization of the lipopolysaccharide induced model of Parkinson's disease: role of oxidative stress and neuroinflammation. Neurochem Int 87: 92–105, 2015
61. Simonyi A, Serfozo P, Lehmidi TM, Cui J, Gu Z, Lubahn DB, Sun AY, and Sun GY. The neuroprotective effects of apocynin. Front Biosci (Elite Ed) 4: 2183–2193, 2012
62. Sloan M, Alegre-Abarrategui J, and Wade-Martins R. Insights into LRRK2 function and dysfunction from transgenic and knockout rodent models. Biochem Soc Trans 40: 1080–1085, 2012
63. Spillantini MG, Crowther RA, Jakes R, Hasegawa M, and Goedert M. alpha-Synuclein in filamentous inclusions of Lewy bodies from Parkinson's disease and dementia with lewy bodies. Proc Natl Acad Sci U S A 95: 6469–6473, 1998
64. Subash S, Essa MM, Al-Adawi S, Memon MA, Manivasagam T, and Akbar M. Neuroprotective effects of berry fruits on neurodegenerative diseases. Neural Regen Res 9: 1557–1566, 2014
65. Subramaniam SR. and Chesselet M-F. Mitochondrial dysfunction and oxidative stress in Parkinson's disease. Prog Neurobiol 0: 17–32, 2013
66. Tansey MG. and Goldberg MS. Neuroinflammation in Parkinson's disease: its role in neuronal death and implications for therapeutic intervention. Neurobiol Dis 37: 510–518, 2010
67. Ulatowski LM. and Manor D. Vitamin E and neurodegeneration. Neurobiol Dis 84: 78–83, 2015
68. Varçin M, Bentea E, Michotte Y, and Sarre S. Oxidative stress in genetic mouse models of Parkinson's Disease. Oxid Med Cell Longev 2012: 624925, 2012
69. Wang J, Silva JP, Gustafsson CM, Rustin P, and Larsson N-G. Increased in vivo apoptosis in cells lacking mitochondrial DNA gene expression. Proc Natl Acad Sci U S A 98: 4038–4043, 2001
70. Wang Q, Qian L, Chen SH, Chu CH, Wilson B, Oyarzabal E, Ali S, Robinson B, Rao D, and Hong JS. Post-treatment with an ultra-low dose of NADPH oxidase inhibitor diphenyleneiodonium attenuates disease progression in multiple Parkinson's disease models. Brain 138: 1247–1262, 2015
71. Xu Q, Shenoy S, and Li C. Mouse models for LRRK2 Parkinson's disease. Parkinsonism Relat Disord 18 Suppl 1: S186–S189, 2012
72. Yakovlev G, Reda T, and Hirst J. Reevaluating the relationship between EPR spectra and enzyme structure for the iron sulfur clusters in NADH:quinone oxidoreductase. Proc Natl Acad Sci U S A 104: 12720–12725, 2007
73. Zielonka J, Cheng G, Zielonka M, Ganesh T, Sun A, Joseph J, Michalski R, O'Brien WJ, Lambeth JD, and Kalyanaraman B. High-throughput assays for superoxide and hydrogen peroxide: design of a screening workflow to identify inhibitors of NADPH oxidases. J Biol Chem 289: 16176–16189, 2014

74. Zielonka J, Sikora A, Adamus J, and Kalyanaraman B. Detection and differentiation between peroxynitrite and hydroperoxides using mitochondria-targeted arylboronic acid. Methods Mol Biol 1264: 171–181, 2015
75. Zielonka J, Zielonka M, VerPlank L, Cheng G, Hardy M, Ouari O, Ayhan MM, Podsiadly R, Sikora A, Lambeth JD, and Kalyanaraman B. Mitigation of NADPH oxidase 2 activity as a strategy to inhibit peroxynitrite formation. J Biol Chem 291: 7029–7044, 2016